Discovery and Period Analysis of Seven Variable Stars

Tom Polakis
Command Module Observatory, 121 W. Alameda Drive, Tempe, AZ 85282; tpolakis@cox.net

Received May 3, 2019; revised May 20, 2019; accepted May 25, 2019

Abstract Tens of thousands of images have been acquired during the course of asteroid photometry observations at Command Module Observatory (MPC V02). Nightly sets of these images were analyzed using a software routine that locates field stars whose brightness shows anomalously high photometric scatter. A total of 32 variable stars were identified by this method, six of which are discoveries. An additional discovery was made serendipitously by noticing variability of a comparison star. Follow-up V-band observations were made for all of these stars, and combined with sparse survey data to perform period analysis and create light curves that are presented in this paper. All seven stars are eclipsing binary systems: four are of type W UMa, two are type β Lyr, and one is an Algol-type. Results have been entered into the International Variable Star Index.

1. Introduction

As of May 2019, the International Variable Star Index (VSX; Watson *et al.* 2014) contained data for more than 600,000 variable stars. Many recent discoveries have been made by data mining, taking advantage of the great wealth of available survey data. Despite the preponderance of these data and automated detection methods, a search for bright variable stars was undertaken with the expectation that they still await discovery.

In a typical night of asteroid photometric observations, two to three hundred images are obtained for several targets. After three years of such observing, nearly 100,000 images have been captured. This paper describes the instrumentation and methods that were employed to locate variable stars in these images. Also discussed are follow-up V-band imaging and analysis augmented by survey data, and the securing of precise periods and determination of variable star types.

2. Instrumentation and methods

2.1. Data acquisition

All of the CCD photometric observations were performed at V02 in Tempe, Arizona. Light pollution brightens the sky at this suburban site by roughly three magnitudes per square arcsecond. Images were taken between June 2017 and April 2019 using a 0.32-m f/6.7 Modified Dall-Kirkham telescope and an SBIG STXL-6303 CCD camera. Since asteroids do not vary significantly in color, a "clear" glass filter was used for all images. Exposure time for all the images was 2 minutes, which is a balance between minimizing photometric errors and providing adequate cadence. The image scale after 2 × 2 binning was 1.76 arcsec/pixel. Images were calibrated using a dozen bias, dark, and flat frames. Flat-field images were made using an electroluminescent panel. Image calibration and alignment was performed using MaxIm DL software (Diffraction Limited 2012).

Despite the nightly motion of asteroids, new field centers were required only every fourth night, since it takes a minor planet more than three nights to traverse the 45' × 30' field of the CCD. The relevant benefit to this work of maintaining the same field is that any variable stars that may be discovered could be followed up with images from the two subsequent nights.

2.2. Data reduction

MPO Canopus (Warner 2019) software was used for its features that are unique to performing photometric measurements of Solar System targets. The software also has a "Variable Star Search" feature, in which standard deviation vs. average magnitude for field stars is plotted using images for a particular field during a single night. Time-series plots of the magnitude of the ensemble of chosen comparison stars are also created to confirm that the standard deviations are not a result of local atmospheric effects. Figure 1 is an example of such a plot. The upward ramp for brighter stars at the left end is caused by the detector entering its non-linear range, while the higher errors at the right end are a result of reduced signal-to-noise ratio for fainter stars. Potential variable stars are found in the middle range of the plot.

False positives greatly outnumber actual variable stars in these plots. Stars too near the edge of the frame, companion stars near the edge of the measuring aperture, extended objects, and clouds are just some of the causes. Therefore, an "eye test" is performed by clicking on each data point, which brings up a time-series plot of that star's magnitude relative to the average of the ensemble of comparison star magnitudes. Those plots with a single outlying point or exhibiting a step change in brightness are quickly rejected. Legitimate variable stars show steady ramps, and curvature at regions of inflection, as shown in the example in Figure 2.

This method was employed for 170 fields, each typically containing between 60 and 80 images for a single night. These targeted searches turned up 32 variable stars, 26 of which were already catalogued in VSX.

One of the seven new variable stars was discovered by the luckier method of using it as a comparison star. Canopus provides a plot that compares the magnitude of each comparison star against the average of the other four in the ensemble. Short-period variables often show up as waviness in the plot that should ideally be flat, as shown in Figure 3. Typically, these variables are found to already be catalogued, but this particular case is a new discovery.

For the newly discovered variable stars, magnitudes from the Clear-filtered discovery images were transformed to Johnson V. For each new variable, magnitudes for an ensemble of five comparison stars were obtained from the APASS DR10

catalogue (Henden *et al.* 2019). Comparison stars are solar colored, with B–V ranging from 0.5 to 0.9. In all but one case, the target variable stars are also in this color range. Rudimentary light curves were created from the discovery images only to confirm periodic variability. Follow-up observing for each variable involved targeted imaging of these variables through a V filter, observing them with the appropriate number of nights and cadences.

3. Results

3.1. Light curve created from solely V02 data using V-band images

Figure 4 is the phased light curve for GSC 01845-00905 using data from only V02. The star was observed on nine nights, during which 634 images were obtained. While the minima are adequately defined, there remains a gap in the data near phase 0.8. The period spectrum is plotted in Figure 5. RMS error of the curve fit is plotted on the vertical axis against period solutions ranging from 2.14 to 2.17 days. Note that it shows multiple aliases, creating an ambiguous period solution. It becomes clear that augmentation by survey data would prove beneficial.

3.2. Period solutions and light curves including survey data

Of the many photometric surveys posting online data, ASAS-SN (Kochanek *et al.* 2017) proved to be the most fruitful for V-band measurements. For each target, hundreds of data points gathered between 2016 and the present were used to augment the V02 data. The zero-point difference between the two datasets typically amounted to 0.050 to 0.100 mag., so those points were shifted in the software by the appropriate amount. The longer time range of data was useful in eliminating any ambiguity in the period spectra, and in greatly increasing the precision of the periods.

The benefit of including ASAS-SN survey data for GSC 01845-00905 is illustrated in Figure 6, which shows the period spectrum with the inclusion of ASAS-SN data. Comparing this plot to Figure 5, it can be seen that the survey data's longer time baseline also results in an unambiguous period solution with greater precision.

Period determination was done using the MPO Canopus Fourier-type FALC fitting method (Harris *et al.* 1989). Pertinent data for all seven variable stars are presented in Table 1. Figures 7 through 13 are phased light curves. The smoothed curves are Fourier fits to the data. The first and last data points for each night are highlighted with circles and boxes, respectively. V02 and ASAS-SN data are identified in the legends.

3.3. Discussion of results

In this section, we discuss the columns appearing in Table 1. Where possible, the primary identification is from the Hubble Guide Star Catalog, Version 1.2 (Morrison *et al.* 2001). Otherwise, the UCAC4 (Zacharias *et al.* 2013) designation is adopted. Precise J2000 coordinates were acquired from Gaia DR2 (Gaia Collab. *et al.* 2016, 2018).

We can identify the types of these variables by simply observing the character of their light curves. The majority of the seven stars are W UMa (EW: Figures 7, 10, 12, 13), whose ellipsoidal components are similarly bright, so the primary and secondary minima are nearly equal. Two stars are β Lyr eclipsing binaries (EB: Figures 9 and 11), in which the components are of different brightness, and the two minima are significantly different. Finally, one star is an Algol-type eclipsing binary (EA: Figure 8). In this case, the light does not vary for a long portion of the period, during which the two stars are not eclipsing.

Period solutions are given in days to a precision of six decimal places, with errors indicated. Range is the difference between maximum and minimum light in the Fourier fit.

Most approaches for determining the epoch of minimum light require dense coverage surrounding the minimum with low data scatter. The ASAS-SN data have too much scatter for this method to be viable. Therefore, a pair of data points with known phase information were located on either side of phase = 0 on the Fourier-fitted curve, and their heliocentric Julian Dates were interpolated to arrive at a result that is estimated to 0.0001 day.

4. Conclusions

Despite the large quantity of catalogued variable stars and the volume of survey data, these discoveries with a small telescope at a suburban site demonstrate that many more bright variable stars await discovery. Follow-up observations done at the appropriate level coupled with photometric survey data yielded precise period solutions and light curves.

Most variable stars having large amplitudes have already been discovered. It is more likely that new discoveries will be of variables with amplitudes of several tenths of a magnitude. This is a common range for eclipsing binary stars, so they are likely candidates for discovery, as was the case for all seven stars in this work.

5. Acknowledgements

The effort was inspired by a presentation by Maurice Clark (Clark 2018), who discovered variable stars using a similar method. The author would like to thank Brian Skiff for his indispensable mentoring in data acquisition and reduction. Thanks also go out to Brian Warner for support of his MPO Canopus software package. Sebastián Otero was responsive and helpful with matters relating to VSX. This research was made possible through the use of the AAVSO Photometric All-Sky Survey (APASS), funded by the Robert Martin Ayers Sciences Fund and NSF AST-1412587.

References

Clark, M. 2018, in *The Society for Astronomical Sciences 37th Annual Symposium on Telescope Science*. Society for Astronomical Sciences, Rancho Cucamonga, CA, 105.

Diffraction Limited. 2012, MAXIMDL image processing software (http://www.cyanogen.com).

Gaia Collaboration, *et al.* 2016, *Astron. Astrophys.*, **595A**, 1.

Gaia Collaboration, *et al.* 2018, *Astron. Astrophys.*, **616A**, 1.

Harris, A. W., *et al.* 1989, *Icarus*, **77**, 171.

Henden, A. A., *et al.* 2019, AAVSO Photometric All-Sky Survey, data release 10 (http://www.aavso.org/apass).

Kochanek, C. S., *et al.* 2017, *Publ. Astron. Soc. Pacific*, **129**, 4502.

Morrison, J. E., Röser, S., McLean, B., Bucciarelli, B., and Lasker, B. 2001, *Astron. J.*, **121**, 1752.

Warner, B. D. 2019, MPO CANOPUS software (http://bdwpublishing.com).

Watson, C., Henden, A. A., and Price, C. A. 2014, AAVSO International Variable Star Index VSX (Watson+, 2006–2014; http://www.aavso.org/vsx).

Zacharias, N., Finch, C. T., Girard, T. M., Henden, A., Bartlett, J. L., Monet, D. G., and Zacharias, M. I. 2013, *Astron. J.*, **145**, 44.

Table 1. Photometry for recently discovered variable stars.

Ident.	*R.A. (J2000.0)* h m s	*Dec. (J2000.0)* ° ‘ “	*Type*	*Period (d)*	*Error (d)*	*Max. (V)*	*Min. (V)*	*Epoch of Min. (HJD)*	*Figure*
GSC 01224-00315	02 56 17.57	+16 35 26.1	EW	0.423042	0.000003	14.02	14.11	2458053.7046	7
GSC 01845-00905	05 05 31.19	+22 43 07.1	EA	2.152089	0.000003	14.37	14.92	2458107.8820	8
GSC 01299-01898	05 45 25.71	+15 22 08.5	EB	0.529882	0.000003	13.24	13.61	2458108.8332	9
GSC 01347-00934	07 26 52.98	+15 14 46.0	EW	0.492463	0.000002	13.70	13.82	2458488.9509	10
UCAC4 522-042119	07 40 07.27	+14 22 33.8	EB	0.713958	0.000002	14.12	14.40	2458158.6820	11
GSC 00790-00941	07 43 33.69	+14 23 49.5	EW	0.235043	0.000001	13.98	14.63	2458151.8873	12
GSC 04963-01164	13 06 41.20	–07 03 39.9	EW	0.445836	0.000001	12.31	12.43	2457542.8621	13

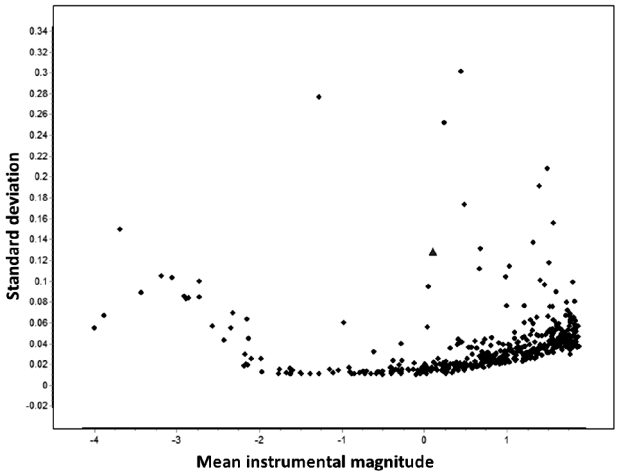

Figure 1. Standard deviation for each catalogued star from 70 images plotted against their mean magnitudes. The triangle identifies variable star GSC 01299-01898, while other outlying points are false positives.

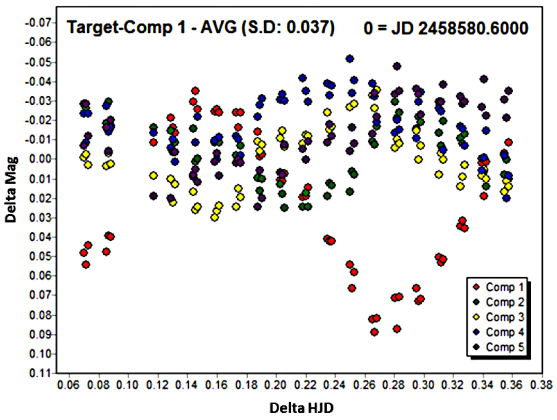

Figure 3. Variation in magnitude of each comparison star relative to the average of the other four. Star #1 (GSC 04963-01164) is clearly variable. Since it is used in the averaging, its variations cause smaller, mirror-image variations of the other four comparison stars.

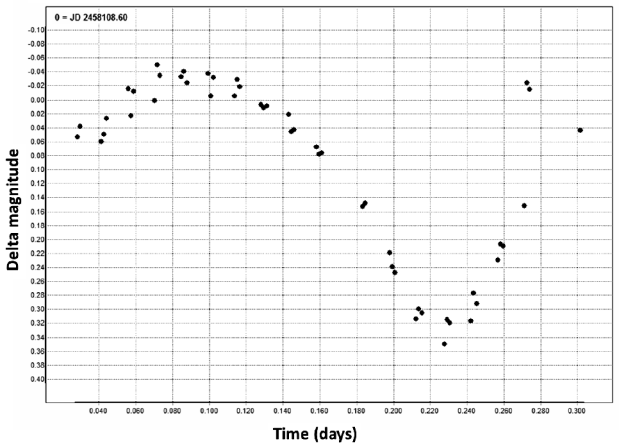

Figure 2. Variation in magnitude of GSC 01299-01898, which was identified in Figure 1

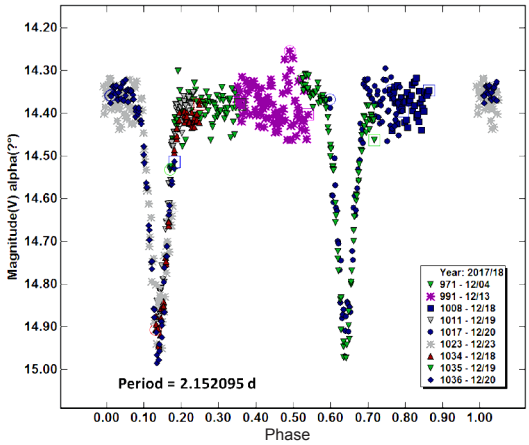

Figure 4. Phased light curve for GSC 01845-00905, using data only from V02.

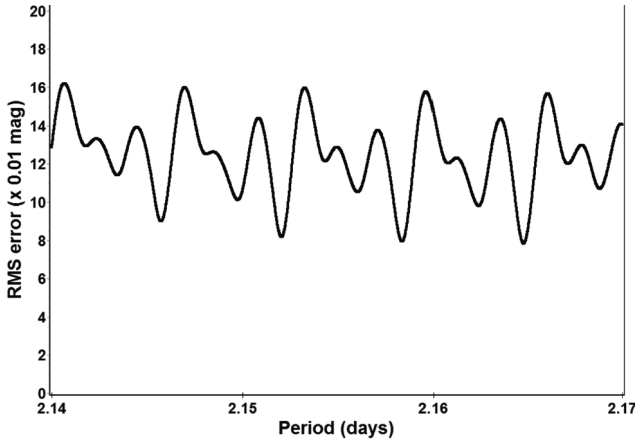

Figure 5. Period spectrum for GSC 01845-00905, using data only from V02. The short time baseline causes multiple aliases between 2.14 and 2.17 days.

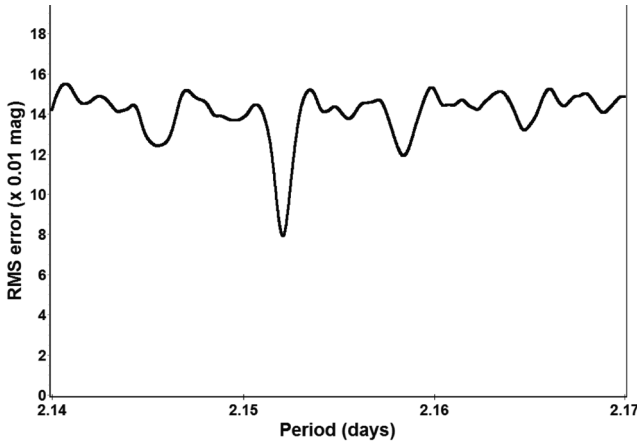

Figure 6. Period spectrum for GSC 01845-00905, using data from both V02 and ASAS-SN survey. Compare with Figure 5. The longer baseline clarifies the period solution.

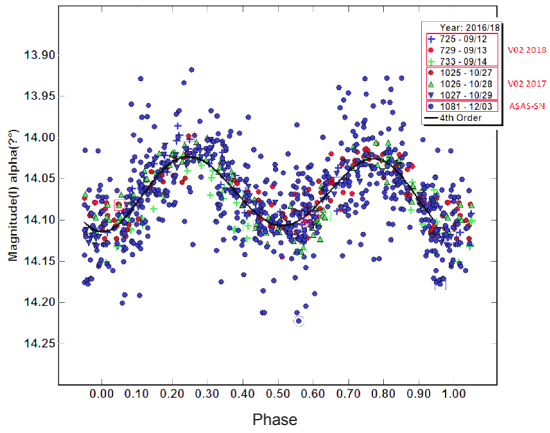

Figure 7. Phased light curve for GSC 01224-00315. Period = 0.423042 d. Epoch of primary minimum = 2458053.7046 HJD.

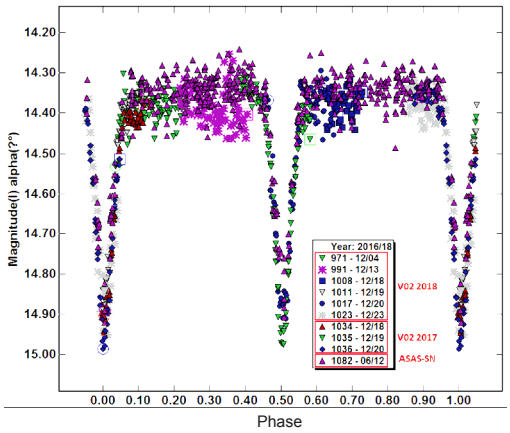

Figure 8. Phased light curve for GSC 01845-00905. Period = 2.152089 d. Epoch of primary minimum = 2458107.8820 HJD.

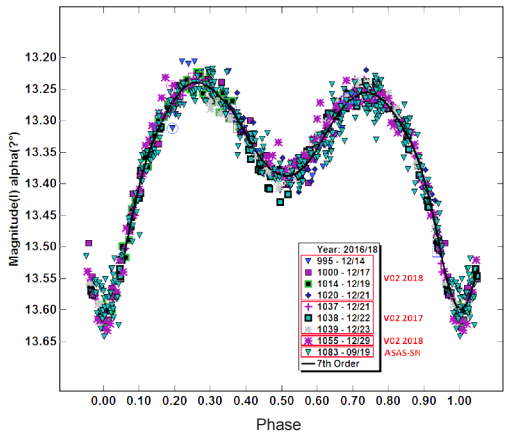

Figure 9. Phased light curve for GSC 01299-01898. Period = 0.529882 d. Epoch of primary minimum = 2458108.8332 HJD.

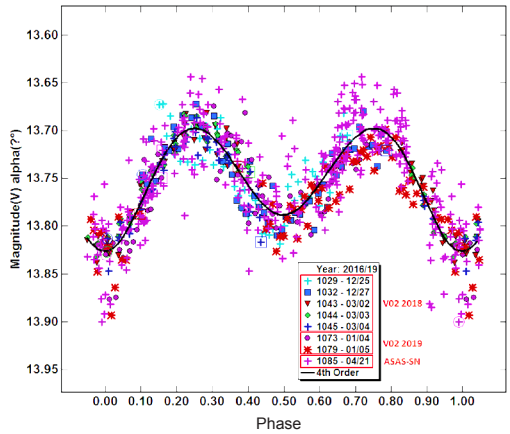

Figure 10. Phased light curve for GSC 01347-00934. Period = 0.492463 d. Epoch of primary minimum = 2458488.9509 HJD.

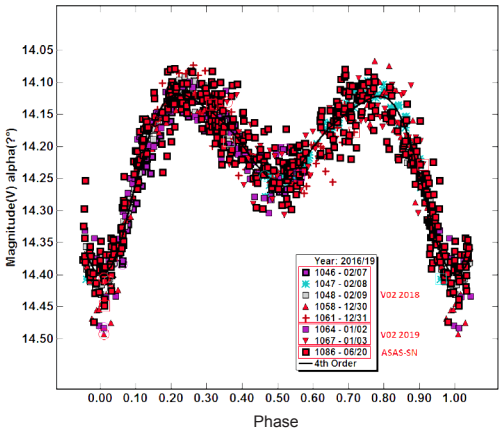

Figure 11. Phased light curve for UCAC4 522-042119. Period = 0.713958 d. Epoch of primary minimum = 2458158.6820 HJD.

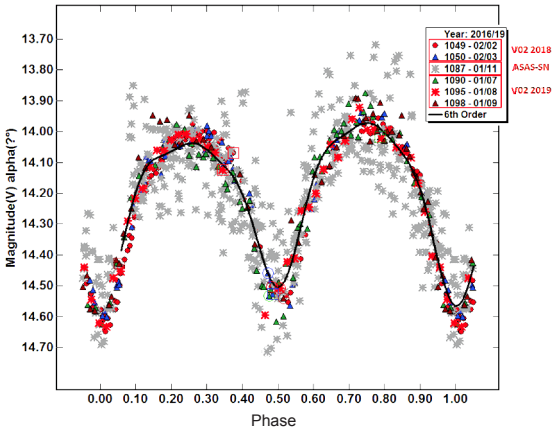

Figure 12. Phased light curve for GSC 00790-00941. Period = 0.235043 d. Epoch of primary minimum = 2458151.8873 HJD.

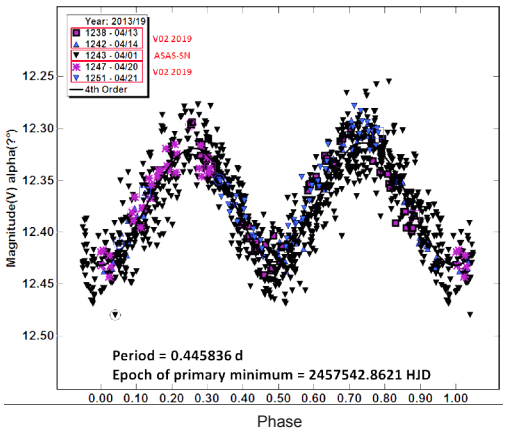

Figure 13. Phased light curve for GSC 04963-01164. Period = 0.445836 d. Epoch of primary minimum = 2457542.8621 HJD.